applied sciences

MDPI

Article

Tunability of Radiation Pattern of the H-Polarized Natural Waves of Dielectric Waveguide with Infinite Graphene Plane and Finite Number of Graphene Strips at THz

Mstyslav E. Kaliberda * and Sergey A. Pogarsky

School of Radiophysics, Biomedical Electronics and Computer Systems, V.N. Karazin Kharkiv National University, 61022 Kharkiv, Ukraine; spogarsky@gmail.com
* Correspondence: kaliberdame@gmail.com

Abstract: We investigate the radiation of the THz natural waves of the dielectric waveguide with graphene plane scattered by finite number of graphene strips. Our mathematically accurate analysis uses the singular integral equations method. The discretization scheme employs the Nystrom-type algorithm. The complex-valued propagation constants of the natural waves and corresponding fields are determined numerically from the equation, which also involves the kernel-function of the singular integral equation. The method we use is meshless and full-wave. The convergence is provided by the mathematical theorems. By varying the chemical potential of graphene and structural geometrical parameters, we examine the elevation angle of the main lobe of the radiation pattern and the radiated power.

Keywords: graphene; integral equation; plasmon wave; leaky-wave antenna

Citation: Kaliberda, M.E.; Pogarsky, S.A. Tunability of Radiation Pattern of the H-Polarized Natural Waves of Dielectric Waveguide with Infinite Graphene Plane and Finite Number of Graphene Strips at THz. *Appl. Sci.* **2023**, *13*, 10563. https://doi.org/10.3390/app131910563

Academic Editors: Mario Lucido, Kazuya Kobayashi, Francisco Medina, Alexander I. Nosich and Elena D. Vinogradova

Received: 21 August 2023
Revised: 15 September 2023
Accepted: 20 September 2023
Published: 22 September 2023

1. Introduction

The ability to tune an antenna's main lobe angle is a desirable property. In leaky-wave antennas, which use the dielectric waveguide as a guiding element and incorporate periodic grating as a scattering object, the period and parameters of the waveguide significantly affect the angle of the main lobe at a certain frequency [1]. The variation of the wavelength of the natural wave (eigenwave) of the waveguide can lead to the variation of the angle of the main lobe. This can be achieved by changing the structural parameters. Another approach is to leave the geometrical parameters unchangeable, but to use material with dynamically controllable properties [2–5]. Graphene is one such material, which has an almost infinitely thin resistive surface with complex-valued conductivity, denoted as $\sigma = \sigma(f, \mu_c, \tau, T)$. The conductivity is a function of four parameters: the frequency f, chemical potential μ_c, electron relaxation time τ and temperature T. The conductivity σ can be controlled dynamically by the application of electrostatic or magnetostatic doping and by changing the chemical potential μ_c. Graphene strips are capable of supporting plasmon-polariton waves and corresponding plasmon resonances in the low THz range. Together with the extraordinary hardness and flexibility of graphene, these properties open up wide opportunities for its inclusion in the construction of tunable antennas, absorbers, sensors, polarizers, lasers, etc. [6–11]. In [12], dynamic single- and dual-channel graphene Q-switching in an Yb:YAG waveguide with controlled power-splitting ratios for application in lasers is demonstrated.

A commonly employed technique for studying the graphene structures is the finite-difference time-domain (FDTD) method with modifications [8,9]. The modifications are proposed due to the mesh size dependency on the size of the scatterers, particularly the thickness of the graphene elements. Given that the graphene is ideally monolayer, extremely dense mesh is need. The finite element method (FEM) is used in [11] to study the graphene-based sensor. FDTD or commercial packages based on FEM use approximate

radiation conditions and do not take into account the edge condition, which limits the accuracy of the results. In [13], a graphene antenna at frequencies up to 0.8 THz is proposed. CST microwave studio analysis software is used for the modelling. In this frequency range, the resonance frequency is only slightly influenced by the chemical potential and almost cannot be controlled by electrostatic or magnetostatic biasing.

Approximate methods allow a solution to be obtained in much less computation time, and some physical effects to be studied analytically, but at the cost of accuracy. In [14], the graphene patch antenna is considered with the use of the equivalent circuit. The omnidirectional radiation pattern is comparable to that of the conventional metal implementations. However, the resonance frequency is controlled by variation of the chemical potential. In [15], the authors study the graphene bowtie antenna properties for different values of chemical potential, arm length, relaxation time and substrate thickness based on the equivalent circuit. In [16], the leaky-wave antennas based on a single dielectric slab and a double dielectric slab, with an infinite graphene plane or infinite graphene strips excited by dipole, are investigated. An approximate solution is obtained. The radiation patterns demonstrate a controllable elevation angle of the main lobe that depends on the chemical potential of the graphene, accompanied by a noticeable reduction in the maximum of the main lobe. Plasmon wave propagation along the infinite graphene strip is considered in [17]. The authors achieved a change in the elevation angle by modulating the value of the chemical potential of the strip according to a sinusoidal law.

Meshless full-wave methods, such as methods of analytical regularization or integral equations, have guaranteed convergence and offer controlled accuracy, limited, in principle, only by the precision of the corresponding programming language, where the home-made code is created. Employing the functional approach of the Riemann–Hilbert problem, in [18] the authors effectively inverse the static part of the scattering operator, which arises in the H-polarized electromagnetic wave diffraction by graphene grating with the dielectric substrate. In [19], after regularization, the set of the integral equations with additional conditions is obtained for the pre-fractal grating of impedance strips. The approach involving the Helmholtz decomposition and the Galerkin method is applied in [20,21] to both single graphene disks and several layers of graphene disks. As a result, second kind Fredholm equations are obtained.

The method of singular integral equations (SIEs) with Nystrom-type discretization schemes is proposed in [22–26] to study the scattering of waves emitted by the magnetic line source by the dielectric cylinder of circular cross section with graphene strips, and of the H-polarized waves by the graphene grating inside the dielectric waveguide. The Nystrom-type algorithms of discretization can be considered as a numerical regularization. The H-polarization case is of interest (vector $\vec{H}$ is parallel to the edges of the strips), because here, unlike in the E-polarization case, plasmon resonances can arise. In this situation, where natural waves are radiated from the dielectric waveguide due to the scattering by graphene strips, as in the case of PEC (perfectly electric conducting) analogs, the elevation angle of the main lobe strongly depends on the excitation frequency and the period. By varying the chemical potential, it is possible to control a number of characteristics, including the radiated power and the side-lobes level at a fixed frequency, as well as to change the plasmon resonance frequency.

In this paper, we consider the radiation of the natural waves of the planar dielectric waveguide with the infinite graphene plane and with the graphene strip grating. The propagation constant characterizing the natural wave directly depends on the conductivity of the graphene plane. Thus, manipulating the chemical potential of this plane will allow us to regulate the main lobe elevation angle of the radiation pattern. Furthermore, by manipulating the chemical potential of graphene strips forming the grating, the radiated power and maximum of the main lobe can be controlled. We should mention that THz generators are piecemeal and not available on an industrial scale. Our purpose is the theoretical study of the influence of the chemical potential on the radiation characteristics with the use of the developed full-wave meshless method.

Here we have two sub-problems. One is determining the propagation constants of the natural waves (eigenwaves) of the dielectric waveguide backed by the infinite graphene plane, which gives a transcendent complex-valued equation. Another is the scattering problem of these natural waves by the system of finite number of graphene strips placed on the waveguide. The solution gives a singular integral equation [27].

For graphene, the following boundary conditions can be used [10]:

$$E_\tau^+ = \frac{1}{\sigma}(H_\tau^+ - H_\tau^-), \tag{1}$$

$$E_\tau^+ = E_\tau^-, \tag{2}$$

where symbols "±" denote the limit values of the field components above (for "+") or below (for "−") the interfaces. The conductivity of graphene σ can be determined using the Kubo formalism [28,29].

Spatial dispersion can be neglected for surface waves propagating along the graphene plane for the considered frequency range and graphene parameters. When spatial dispersion is taken into account, one more type of mode appears. However it is extremely lossy in the band of interest, which greatly limits its use in practical applications and it is not considered in our paper [30].

2. Solution to the Scattering Problem

Let us consider a planar dielectric waveguide characterized by a width h, with infinite graphene plane at $z = -h$ and finite number of graphene strips at $z = 0$. The finite set of infinite graphene along the x-axis strips we denote as $L = \bigcup_{n=1}^{N} L_n$, where N is the number of strips and L_n is the nth strip. The relative permittivity of the dielectric is ε. The scattering geometry and notations are presented in Figure 1. The time dependence $\exp(-i\omega t)$ is omitted, where ω is the angular frequency.

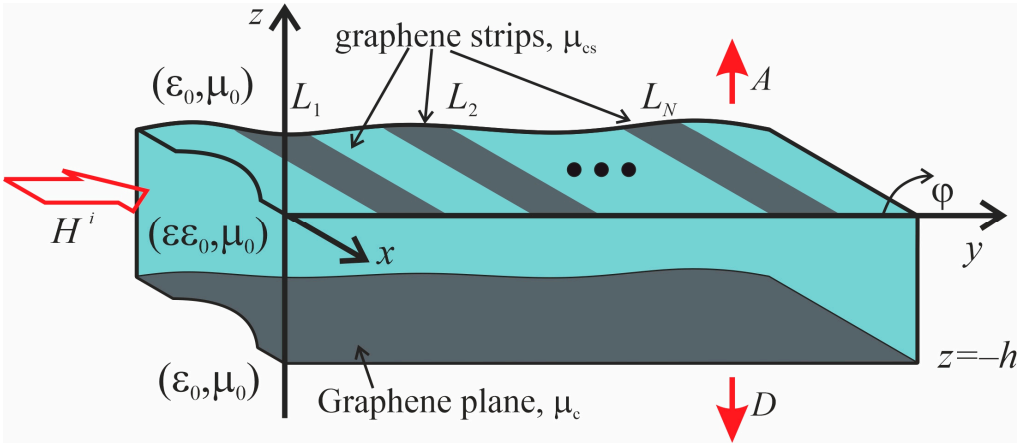

Figure 1. Structure geometry.

We consider the H-polarized incident natural waves of the waveguide, which propagate from the domain $y < 0$ to $y = +\infty$. The total field is a superposition of the incident field, denoted as H^i, and scattered field, denoted as H^s:

$$H^t = H^i + H^s. \tag{3}$$

The field is the solution of the Helmholtz equation, with boundary conditions on and outside graphene (1) and (2), and

$$H_x^+ = H_x^-, \text{ outside ographene,} \tag{4}$$

the radiation and the edge conditions. It is important to mention that this boundary-value problem has a unique solution.

Both the incident field and the scattered field are currently unknown. We use the decomposition of the scattered field with the help of Fourier integrals with unknown amplitudes

$$H^s = \begin{cases} \int\limits_{-\infty}^{\infty} A(\theta)\exp(iky\theta + ikz\gamma(\theta))d\theta, & z > 0, \\ \int\limits_{-\infty}^{\infty} (B(\theta)\exp(ik_1y\theta + ik_1z\gamma(\theta)) + C(\theta)\exp(ik_1y\theta - ik_1z\gamma(\theta)))d\theta, & -h < z < 0, \\ \int\limits_{-\infty}^{\infty} D(\theta)\exp(ik\theta y - ik\gamma(\theta)z)d\theta, & z < -h, \end{cases} \tag{5}$$

where $k = 2\pi/\lambda$ and $k_1 = \sqrt{\varepsilon}k$ are wave numbers in vacuum and inside the dielectric, $\gamma(\theta) = \sqrt{1-\theta^2}$ with the following branch: if $\mathrm{Im}\gamma = 0$ then $\mathrm{Re}\gamma \geq 0$; if $\mathrm{Re}\gamma = 0$ then $\mathrm{Im}\gamma \geq 0$. The field expressed by (5) satisfies the radiation condition. Inside the waveguide, the field can be expressed with the help of the sum of its natural waves. From the mathematical point of view, it means that functions $A(\theta)$, $B(\theta)$, $C(\theta)$ and $D(\theta)$ have singularities in the form of poles. The poles are located at the points, which coincide with the propagation constants of the natural waves.

Enforcement of the boundary conditions (1), (2) and (4), if $z = -h$ and $z = 0$, gives the following dual integral equation

$$\int\limits_{-\infty}^{\infty} C_1(\theta)\exp(ik_1y\theta)d\theta = 0, \quad y \notin L, \tag{6}$$

$$ik_1\int\limits_{-\infty}^{\infty} \Gamma(\theta)C_1(\theta)\exp(ik_1y\theta)d\xi + \frac{ik(\varepsilon+1)}{\sigma Z}\int\limits_{-\infty}^{\infty} C_1(\theta)\exp(ik_1y\theta)d\xi = -\frac{(\varepsilon+1)}{\varepsilon}\frac{\partial H^{inc}}{\partial z}, \quad y \in L, \tag{7}$$

where

$$\Gamma(\theta) = \frac{\varepsilon+1}{\varepsilon}\gamma(\theta)\frac{b(\theta)-1}{a(\theta)-b(\theta)-1}, \tag{8}$$

$$A(\theta) = \frac{a(\theta_1)C_1(\theta_1)/\sqrt{\varepsilon}}{a(\theta_1)-b(\theta_1)-1}, \tag{9}$$

$$B(\theta) = \frac{b(\theta)C_1(\theta)}{a(\theta)-b(\theta)-1}, \tag{10}$$

$$C(\theta) = \frac{C_1(\theta)}{a(\theta)-b(\theta)-1}, \tag{11}$$

$$D(\theta) = \frac{d(\theta_1)C_1(\theta_1)/\sqrt{\varepsilon}}{a(\theta_1)-b(\theta_1)-1}, \tag{12}$$

$$\begin{aligned} a(\theta) = {} & \tfrac{2\gamma(\theta)}{\gamma(\theta\sqrt{\varepsilon})\sqrt{\varepsilon}\Theta(\theta)} \\ & \times\big(ik_1\gamma(\theta)(1+\gamma(\theta\sqrt{\varepsilon})\sigma Z)\sin(k_1h\gamma(\theta))) - k_1\gamma(\theta\sqrt{\varepsilon})\sqrt{\varepsilon}\cos(k_1h\gamma(\theta))\big), \end{aligned} \tag{13}$$

$$b(\theta) = \frac{\exp(ik_1h\gamma(\theta))k_1(\gamma(\theta)+\gamma(\theta)\gamma(\theta\sqrt{\varepsilon})\sigma Z - \gamma(\theta\sqrt{\varepsilon})\sqrt{\varepsilon})}{\Theta(\theta)}, \tag{14}$$

$$d(\theta) = \frac{2k_1\gamma(\theta)\exp(-ik_1h\gamma(\theta\sqrt{\varepsilon}))}{\Theta(\theta)}, \tag{15}$$

$$\Theta(\theta) = \exp(-ik_1 h\gamma(\theta))k_1(\gamma(\theta) + \gamma(\theta)\gamma(\theta\sqrt{\varepsilon})\sigma Z + \gamma(\theta\sqrt{\varepsilon})\sqrt{\varepsilon}), \tag{16}$$

$\theta_1 = \theta/\sqrt{\varepsilon}$, $C_1(\theta)$ is an unknown function and $Z = 120\pi\Omega$ is the impedance of free space. To find $C_1(\theta)$, we reduce (6) and (7) to an SIE.

We should note that $\Gamma(\theta)$ possesses the following asymptotic relation: $\Gamma(\theta) \sim i|\theta| - \frac{i}{2|\theta|}\frac{(1+\varepsilon+\varepsilon^2+\varepsilon^3)}{\varepsilon(1+\varepsilon)^2} + O(|\theta|^{-3})$, if $\theta \to \infty$. As one can see, the first term is increasing and all others are decreasing. To the increasing integrand in (6), we use the parametric representation of the Hilbert pseudo-differential operator [31] and reduce it to the singular integral. For all non-increasing terms, we collect to the regular part of the kernel-function $K(y, \xi)$. As a result, the following SIE of the first kind with additional conditions can be obtained:

$$\frac{1}{\pi} PV \int_L K(y,\theta)G(\theta)d\xi = -\frac{(\varepsilon+1)}{\varepsilon}\frac{\partial H^{inc}}{\partial z}, \quad y \in L, \tag{17}$$

$$\frac{1}{\pi}\int_{L_m} G(\theta)d\theta = 0, \quad m = 1,\ 2,\ \ldots,\ N, \tag{18}$$

where $G(y) = ik_1 \int_{-\infty}^{\infty} \theta C_1(\xi)\exp(ik_1\theta y)d\xi$ is Fourier transform of $C_1(\theta)$ with factor $ik_1\theta$. $F(y)$ is up to the constant the currents density on graphene strips. The kernel-function is

$$K(y,\theta) = \frac{1}{\theta - y} + ik_1\int_0^{\infty} \frac{(\eta + i\Gamma(\eta))\sin(k_1\eta(y-\theta))}{\eta}d\eta + \begin{cases} ik(\varepsilon+1)\pi(\sigma Z_0)^{-1}, & if \quad \xi \le y, \\ 0, \quad if \quad \xi > y, \end{cases} \tag{19}$$

and the first term in (19) is singular one. All other terms are regular. We should note that the second term in (7) equals $G(y)$ (with the constant factor). However, we collect to the kernel-function as the third term in (19) to obtain an SIE of the first kind rather than the second kind.

Based on the corresponding theorems, we can state that the solution of (17) and (18) is unique [32]. To carry out the discretization process, the Nystrom-type method is employed [26]. From the edge condition it follows that unknown function $G(\theta)$ has inverse square root singularities at the edges of the strips. Thus, the appropriate quadrature rule with nodes at the zeros of the Chebyshev polynomials of the first kind is applied, while the collocation points are the zeros of the Chebyshev polynomials of the second kind. Theorems formulated in [32] confirm the convergence.

3. Solution to the Natural Waves Problem

Let us consider natural waves, which propagate from the region $y = -\infty$ in the direction of $y = +\infty$. The y-dependence is $\exp(ik\beta|y|)$. $\mathrm{Re}\beta > 0$ and $\mathrm{Im}\beta > 0$, β are unknown propagation constants of the natural wave. As the graphene conductivity is a complex-valued function, the graphene plane absorbs the electromagnetic field and the propagation constants are complex values.

To obtain the field of natural wave, one can represent it as plane waves in each domain $z > 0$, $0 > z > -h$ and $z < -h$ [33]:

$$H_x = \begin{cases} e\exp(ikz\gamma(\beta)), & z > 0, \\ f\cos(k_1 z\gamma(\beta/\sqrt{\varepsilon})) + \sin(ik_1 z\gamma(\beta/\sqrt{\varepsilon})), & 0 > z > -h, \\ g\exp(-ikz\gamma(\beta)), & z < -h. \end{cases} \tag{20}$$

The term $\exp(ik\beta|y|)$ is omitted. For the square root, we take the branch $\mathrm{Re}\gamma < 0$ or $\mathrm{Im}\gamma > 0$. Then the amplitude of the field vanishes if $y \to \infty$ or $|z| \to \infty$.

After enforcement of the boundary conditions on the graphene plane (1) and (2), as well as at the vacuum-dielectric interface (2) and (4), one can obtain relationships between amplitudes in each domain and the transcendental equation relatively propagation constant.

As mentioned above, the Fourier amplitudes in (5) and, consequently, the terms within the integral in (19), have poles at the points, which we denoted as β. Thus the equation relatively propagation constant is

$$\frac{(\eta + i\Gamma(\eta))\sin(k_1\eta(y-\theta))}{\eta} = \infty \tag{21}$$

or

$$a(\theta) - b(\theta) - 1 = 0. \tag{22}$$

4. Numerical Results

4.1. Study of Natural Waves

The numerical solution of (22) and the transcendental equation obtained from (20) after application of the boundary conditions are identical. This can be considered as numerical validation.

The studied waveguide consists of two sub-structures, which support natural waves. One is a dielectric waveguide. The other is an infinite graphene plane. The set of natural waves splits into two families, which correspond to each sub-structure. We denote them as H_1 and P_1. Such splitting is also observed in other types of dielectric structures covered with graphene (see, for example, [34]). Figures 2 and 3 show propagation constants of the dominant (in the H-polarization case) natural waves H_1 and P_1 vs. the frequency for various values of the chemical potential and two values of the width of the dielectric slab, which forms the waveguide. Wave H_1 is the natural wave of the dielectric waveguide, which experiences slight perturbation because of the presence of the graphene plane. Wave P_1 is a plasmon natural wave. Its propagation constant significantly depends on the value of the chemical potential and is almost independent on the width of the dielectric slab. Field distribution of these two waves is represented in Figure 4. The waveguide walls are shown as vertical green lines. The electric and magnetic fields of plasmon wave P_1 have visible maximum near the graphene plane; this is surface wave, which propagates along the graphene sheet. Magnetic field of H_1 has maximum approximately at the center of the waveguide.

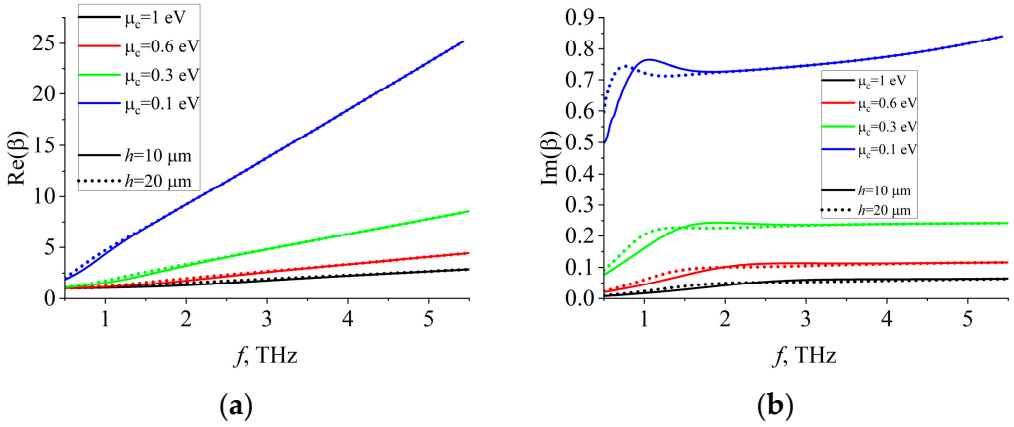

(**a**) (**b**)

Figure 2. Dependences of the propagation constant of the plasmon natural wave P_1 on the frequency, $\varepsilon = 2.25$. (**a**) Real part; (**b**) Imaginary part.

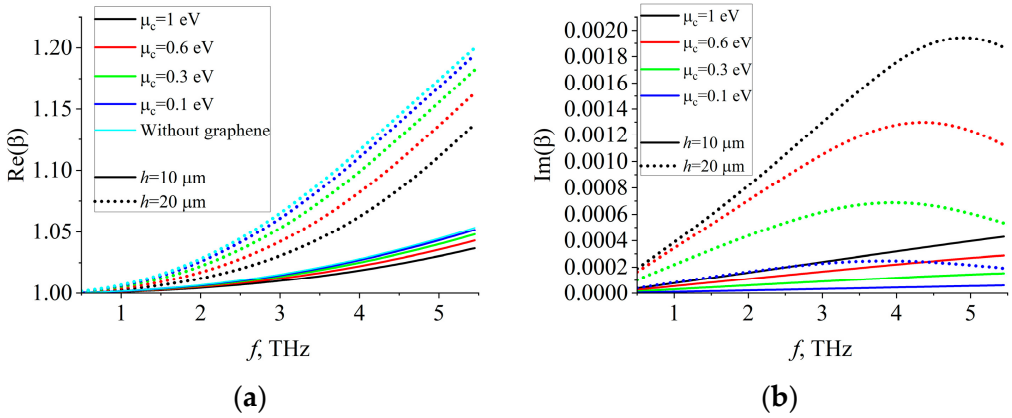

Figure 3. Dependences of the propagation constant of the natural wave H_1 on the frequency, $\varepsilon = 2.25$. (**a**) Real part; (**b**) Imaginary part.

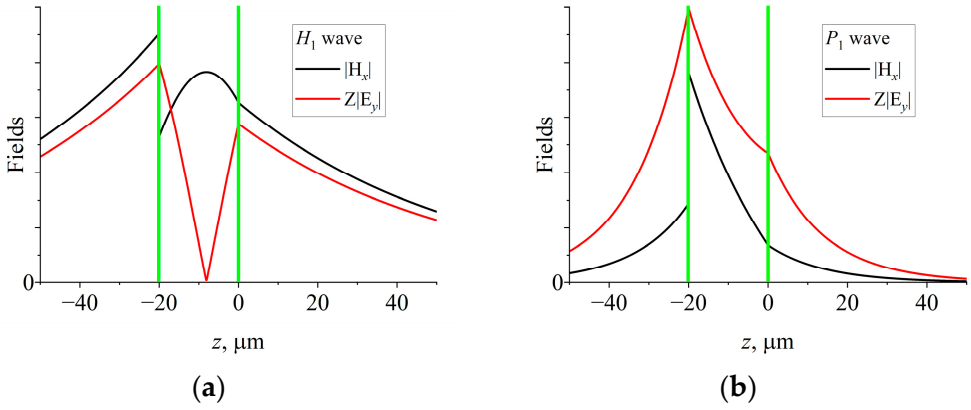

Figure 4. Field distribution of the natural waves (**a**) H_1 and (**b**) P_1, $\varepsilon = 2.25$, $h = 20$ μm, $\mu_c = 0.6$ eV and $f = 2$ THz. (**a**) H_1 natural wave; (**b**) P_1 natural wave.

The strong dependence of the plasmon wave propagation constant on the chemical potential makes it preferable in our further analysis of the tunable properties of the waveguide loaded with graphene strips.

4.2. Scattering of the Natural Waves

Let us consider the scattering of the natural wave P_1. The maximum of the fields of plasmon wave is concentrated near the graphene plane. The amplitude vanishes exponentially when moving away from the graphene plane. To obtain effective coupling of this wave with graphene strips, the width of the dielectric waveguide should be minimal.

The graphene is able to absorb the electromagnetic field. The amplitude of the natural waves of the waveguide decreases if y increases. We suppose that incident natural wave has unit power at the edge of the first graphene strip.

Let us denote the chemical potential of the strips as μ_{cs}. The chemical potential of the graphene plane is, as before, μ_c. Figures 5–7 show dependences of the radiated power on the frequency in the case of P_1 natural wave incidence. The number of strips is taken so that the incident wave is almost attenuated along the length of the structure at the frequency band of interest, $N = 5$. In periodic gratings with dielectric substrate, the grating-mode (or lattice-mode) resonances can arise [18,23–26]. Their frequency depends on material parameters of the substance of the waveguide and the period. Near these resonances, minima of the radiation are observed. The current distribution is in-phase on the strips. The maximum of radiation is at $\varphi = 90°$. At the frequencies higher than the frequency of the grating-mode resonance, the second lobe appears. We denote the first such resonance

as G_1. Graphene strips are capable of maintaining plasmon resonances within the THz range. Their frequency is influenced by the parameters of graphene strips, including width and conductivity. Near plasmon resonances, the maxima of the radiation are observed. As one can see in Figures 5–7, in the case of simultaneous excitation of the plasmon and G_1 resonances, the radiation level still significantly decreases. Thus, the preferable frequency band is near the plasmon resonances but up to G_1.

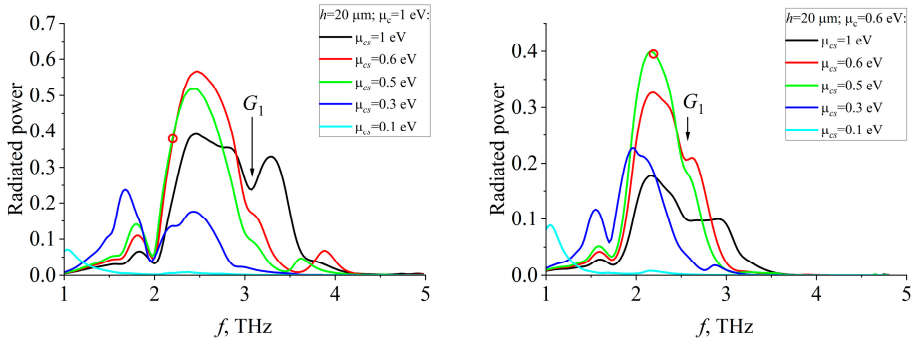

Figure 5. Dependences of the radiated power on the frequency for $h = 20$ μm, $d = 10$ μm, $l = 50$ μm, $N = 5$, $\varepsilon = 2.25$ and P_1 natural wave incidence, (**a**) $\mu_c = 1$ eV; (**b**) $\mu_c = 0.6$ eV. The circles show the value of the frequency for which the radiation patters will be presented.

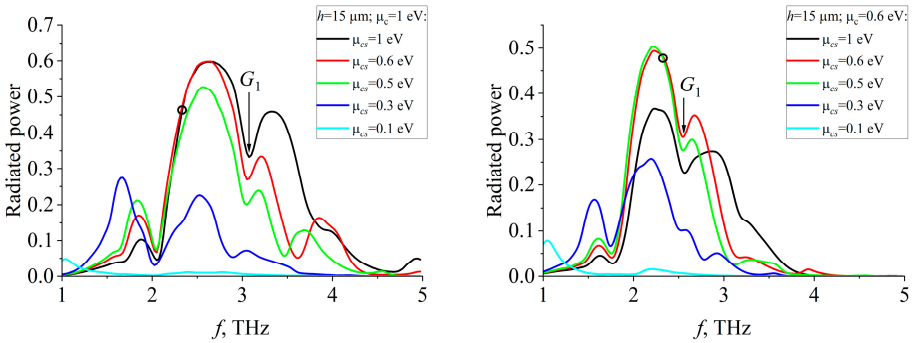

Figure 6. Same study as in Figure 5, but for $h = 15$ μm, (**a**) $\mu_c = 1$ eV; (**b**) $\mu_c = 0.6$ eV.

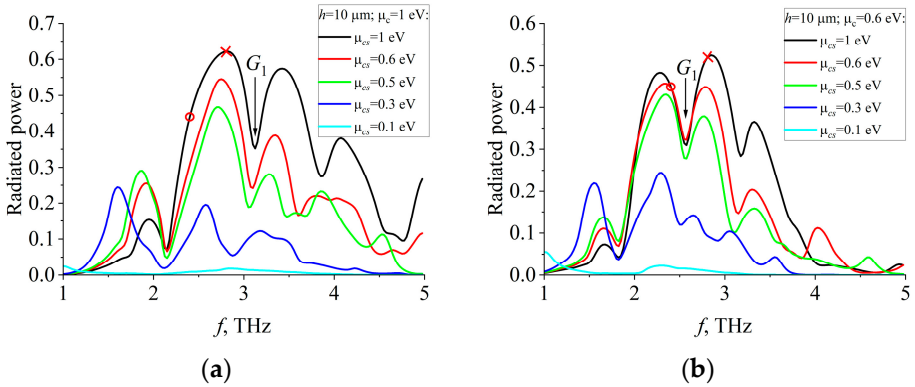

Figure 7. Same study as in Figures 5 and 6, but for $h = 10$ μm, (**a**) $\mu_c = 1$ eV; (**b**) $\mu_c = 0.6$ eV.

If we change the value of the chemical potential of the infinite graphene plane, the propagation constant and, as a result, the resonance frequency of G_1 is also changed. With the decrease in the chemical potential of infinite graphene plane, the attenuation constant of plasmon mode and the absorption of the transferred power increases. The chemical

potential of graphene can be manipulated by electrostatic field application. However, for thin dielectric slab, the field applied to the infinite graphene plane can also affect chemical potential of graphene strips. At present, realistic values of the chemical potential of graphene are from 0 eV up to 1 eV. These considerations prompted us to take the chemical potential of the infinite graphene plane in the interval 0.6 . . . 1 eV.

Figures 8–10 show normalized radiation patterns (in amplitude) for different values of the chemical potential of graphene. For clarity, in Figure 10, we also show the polar plot. The value $\varphi = 0^\circ$ corresponds to the direction of the incidence of the wave. The values of the frequency are taken so that the radiated power is almost the same for $\mu_c = 0.6$ eV and $\mu_c = 1$ eV (see Figures 5–7, marked as circles). By manipulating the chemical potential of the strips, we control the radiated power, as in the case without graphene plane [23,24]. However, manipulating the chemical potential of the infinite graphene plane enables us to change the main lobe elevation angle of the radiation patterns. In the considered case, the width of the interval of variation of the elevation angle is about 35°. A further decrease in the graphene plane chemical potential μ_c results in the noticeable decrease in the radiated power because of absorption of the natural wave during its propagation.

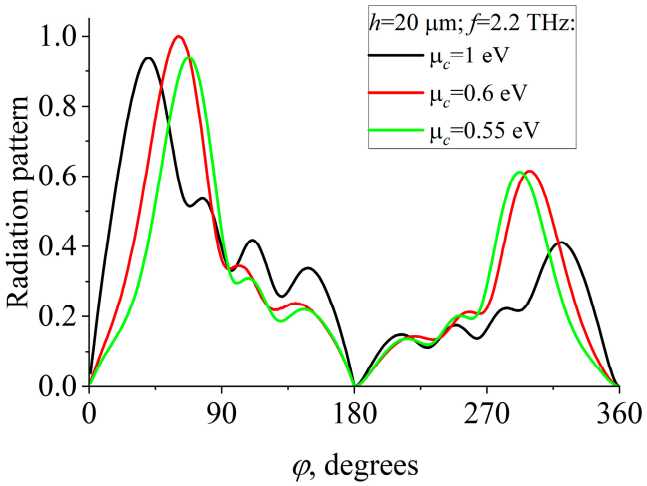

Figure 8. Normalized radiation patterns (in amplitude) for $h = 20$ μm, $f = 2.2$ THz, $\mu_{cs} = 0.5$ eV, $d = 10$ μm, $l = 50$ μm, $N = 5$, $\varepsilon = 2.25$ and P_1 natural wave incidence.

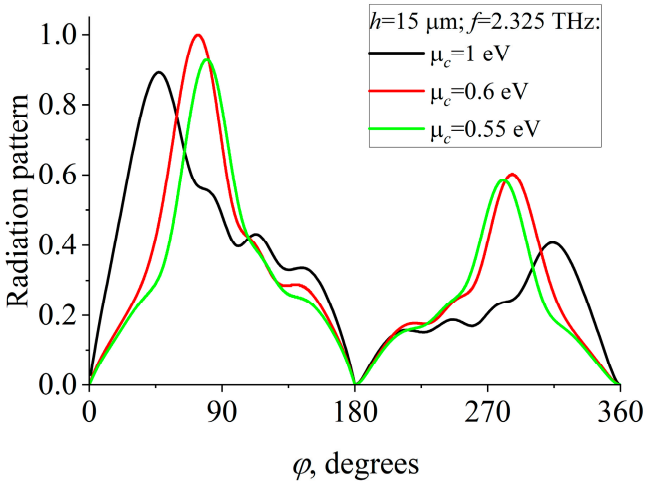

Figure 9. Normalized radiation patterns (in amplitude) for $h = 15$ μm, $f = 2.325$ THz, $\mu_{cs} = 0.6$ eV, $d = 10$ μm, $l = 50$ μm, $N = 5$, $\varepsilon = 2.25$ and P_1 natural wave incidence.

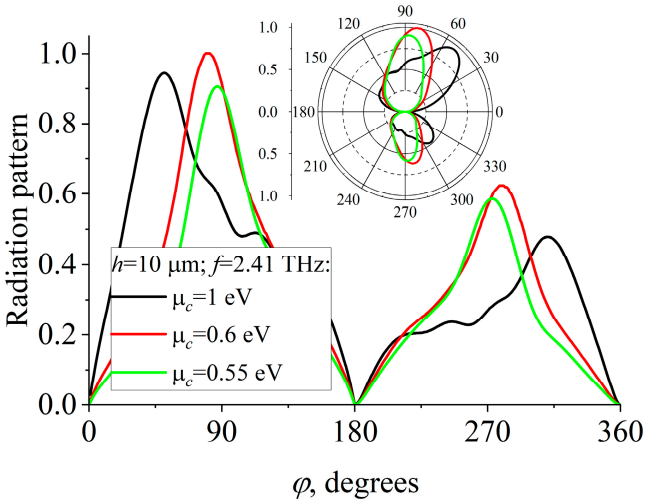

Figure 10. Normalized radiation patterns (in amplitude) for $h = 10$ μm, $f = 2.41$ THz, $\mu_{cs} = 1$ eV, $d = 10$ μm, $l = 50$ μm, $\varepsilon = 2.25$ and P_1 natural wave incidence.

In Figures 8–10, for $0° < \varphi < 180°$ (in the domain above the waveguide), the increase in the chemical potential of graphene plane leads to a leftward shift of the left peak. For $180° < \varphi < 360°$ (in the domain below the waveguide), the increase in the chemical potential leads to a rightward shift of the peak. It can be explained if one considers $\mathrm{Re}(\beta)$ at a fixed frequency for different values of the chemical potential of the graphene plane (see Figure 3a). $\mathrm{Re}(\beta)$ decreases monotonically as μ_c increases. Additionally, as one can observe from Figures 5–7, the position of the grating-mode resonance, for which the current distribution is in-phase on the strips and the elevation angle of the main lobe is 90°, tends to be at the higher values of the frequency.

Rotation angle value can be increased if we consider a frequency greater than the frequency of the resonance G_1. Figure 11 shows normalized radiation patterns (in amplitude) for a relatively small width of the waveguide, $h = 10$ μm. Here, the width of the variation interval of the main lobe is about 46° for $\mu_c = 0.6 \ldots 1$ eV. For such value of the slab width, the decrease in the amplitude of the main lobe is not significant near resonance G_1. Resonance G_1 rises for $\mu_c \approx 0.77$ eV.

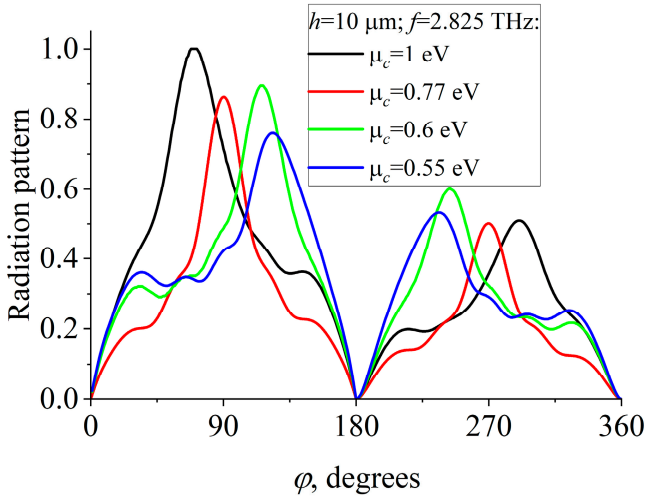

Figure 11. Normalized radiation patterns (in amplitude) for $h = 10$ μm, $f = 2.825$ THz, $\mu_{cs} = 1$ eV, $d = 10$ μm, $l = 50$ μm, $N = 5$, $\varepsilon = 2.25$ and P_1 natural wave incidence.

Finally, in Figure 12 we presented normalized radiation patterns (in amplitude) for the case of the natural wave H_1 incidence. As the attenuation of this wave is much lower than

that of wave P_1, it makes sense to choose a larger number of strips, $N = 20$. The propagation constant of the wave H_1 slightly depends on the chemical potential of graphene plane. As a result, the elevation angle of the main lobe is nearly independent of the chemical potential.

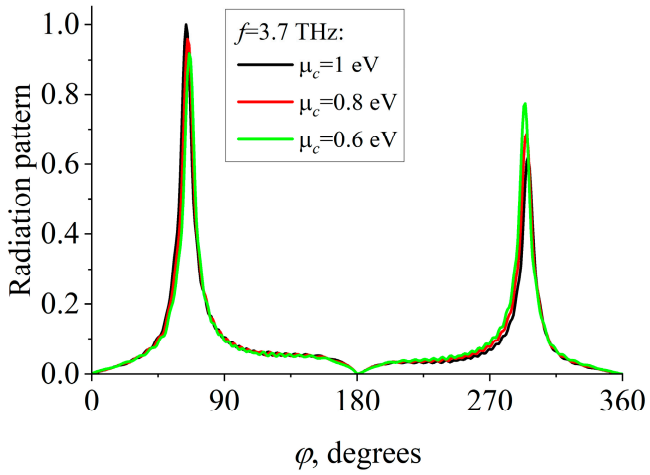

Figure 12. Normalized radiation patterns (in amplitude) for $h = 40$ μm, $f = 3.7$ THz, $\mu_{cs} = 1$ eV, $d = 10$ μm, $l = 50$ μm, $N = 20$, $\varepsilon = 2.25$ and H_1 natural wave incidence.

Our study shows that the influence of the temperature T on the scattering characteristics is negligible.

5. Conclusions

The scattering of the H-polarized natural waves of the dielectric waveguide with graphene plane by finite number of graphene strips and complex-valued eigenvalue problem is considered. The Nystrom-type method of discretization of the singular integral equation is used. Our solution is full-wave and meshless. The convergence is guaranteed by the corresponding theorems.

The ensemble of natural waves of the considered waveguide divides into two distinct categories: plasmon waves, which exhibit the fields compressed to the infinite graphene plane, and waves of dielectric waveguide, which experience slight perturbation by the graphene plane. The propagation constant of the plasmon wave demonstrates significant dependence on the chemical potential. This wave, scattered by the finite number of graphene strips, forms a tunable radiation pattern. The manipulation of the chemical potential of the graphene strips enables us to control the radiated power. The variation of the chemical potential of the infinite graphene plane allows us to control the main lobe elevation angle. Depending on the width of the dielectric slab, in the considered cases the width of the interval of variation of the main lobe elevation angle is about 35° or 46°. Taking into account the exponential decay of the field of the plasmon natural wave in the transverse direction, it is desirable to use a thin dielectric substrate. The frequency band should be chosen near the first plasmon resonance arising on the graphene strips, as this is where the radiation is maximal.

The further analysis can focus on the multilayer system. Considering that unbiased graphene is almost transparent and that the elevation angle of the main lobe depends on the period, graphene layers of strip gratings with different periods can be considered to further increase the range of angle variation.

Author Contributions: Methodology, M.E.K.; software, M.E.K.; validation, M.E.K. and S.A.P.; formal analysis, M.E.K. and S.A.P.; writing—original draft preparation, M.E.K.; writing—review and editing, S.A.P. All authors have read and agreed to the published version of the manuscript.

Funding: S.A.P. obtained funds from the Ministry of Education and Science of Ukraine, grants number 0122U001486, 0122U001436, M.E.K. thanks the National Research Foundation of Ukraine for support under Project 2020.02.0150.

Institutional Review Board Statement: Not applicable.

Informed Consent Statement: Not applicable.

Data Availability Statement: The authors provide equations that can be implemented with the home-made code, enabling the reproduction of all the presented results.

Conflicts of Interest: The authors declare no conflict of interest.

References

1. Ghaderi, M.; Bhattacharyya, A. Investigations on planar periodic structures with uniform microstrip lines. *Microw. Opt. Technol. Lett.* **1990**, *3*, 370–372. [CrossRef]
2. Tamagnone, M.; Gomez-Diaz, J.S.; Mosig, J.R.; Perruisseau-Carrier, J. Reconfigurable THz plasmonic antenna concept using a graphene stack. *Appl. Phys. Lett.* **2012**, *101*, 214102. [CrossRef]
3. Fallah, A.; Camacho, M.; Engheta, N. Electron-Sheet Metasurfaces for Reconfigurable Beam Patterns. *IEEE Antennas Wirel. Propag. Lett.* **2022**, *21*, 2201–2205. [CrossRef]
4. Soleimani, H.; Oraizi, H. A novel 2D leaky wave antenna based on complementary graphene patch cell. *J. Phys. D Appl. Phys.* **2020**, *53*, 255301. [CrossRef]
5. Jiang, H.; Cao, X.; Liu, T.; Jidi, L.; Li, S. Reconfigurable leaky wave antenna with low sidelobe based on spoof surface plasmon polariton. *Int. J. Electron. Commun.* **2022**, *157*, 154394. [CrossRef]
6. Mishra, R.; Sahu, A.; Panwar, R. Cascaded graphene frequency selective surface integrated tunable broadband terahertz metamaterial absorber. *IEEE Photonics J.* **2019**, *11*, 2200310. [CrossRef]
7. Nejat, M.; Nozhat, N. Ultrasensitive THz refractive index sensor based on a controllable perfect MTM absorber. *IEEE Sens. J.* **2019**, *19*, 10490–10497. [CrossRef]
8. Zhai, M.-L.; Li, D.-M. Tunable hybrid metal–graphene frequency selective surfaces based on split-ring resonators by leapfrog ADI-FDTD method. *Micro Nano Lett.* **2018**, *13*, 1276–1279. [CrossRef]
9. Chen, J.; Xu, N.; Zhang, A.; Guo, J. Using dispersion HIE-FDTD method to simulate the graphene-based polarizer. *IEEE Trans. Antennas Propagat.* **2016**, *64*, 3011–3017. [CrossRef]
10. Herasymova, D.O.; Dukhopelnykov, S.V.; Natarov, D.M.; Zinenko, T.L.; Lucido, M.; Nosich, A.I. Threshold conditions for transversal modes of tunable plasmonic nanolasers shaped as single and twin graphene-covered circular quantum wires. *Nanotechnology* **2022**, *33*, 495001. [CrossRef]
11. Seyyedmasoumian, S.; Attariabad, A.; Farmani, A. FEM analysis of a λ3/125 high sensitivity graphene plasmonic biosensor for low hemoglobin concentration detection. *Appl. Opt.* **2022**, *61*, 120–125. [CrossRef] [PubMed]
12. Bae, J.E.; Calmano, T.; Kränkel, C.; Rotermund, F. Controllable dynamic single- and dual-channel graphene q-switching in a beam-splitter-type channel waveguide laser. *Laser Photonics Rev.* **2022**, *16*, 2100501. [CrossRef]
13. Kushwaha, R.K. Reconfigurable GNR based elliptical dielectric resonator antenna for THz band applications. *Results Opt.* **2023**, *10*, 100354. [CrossRef]
14. Goyal, R.; Vishwakarma, D.K. Design of a graphene-based patch antenna on glass substrate for high-speed terahertz communications. *Microw. Opt. Technol. Lett.* **2018**, *60*, 1594–1600. [CrossRef]
15. Zhang, B.; Zhang, J.; Liu, C.; Wu, Z.; He, D. Equivalent resonant circuit modeling of a graphene-based bowtie antenna. *Electronics* **2018**, *7*, 285. [CrossRef]
16. Fuscaldo, W.; Burghignoli, P.; Baccarelli, P.; Galli, A. Complex mode spectra of graphene-based planar structures for THz applications. *J. Infrared Millim. Terahertz Waves* **2015**, *36*, 720–733. [CrossRef]
17. Esquius-Morote, M.; Gomez-Diaz, J.S.; Perruisseauz-Carrier, J. Sinusoidally modulated graphene leaky-wave antenna for electronic beamscanning at THz. *IEEE Trans. Terahertz Sci. Technol.* **2014**, *4*, 116–122. [CrossRef]
18. Yevtushenko, F.O.; Dukhopelnykov, S.V.; Zinenko, T.L.; Rapoport, Y.G. Electromagnetic characterization of tuneable graphene-strips-on-substrate metasurface over entire THz range: Analytical regularization and natural-mode resonance interplay. *IET Microw. Antennas Propag.* **2021**, *15*, 1225–1239. [CrossRef]
19. Koshovy, G.I. The Cauchy method of analytical regularisation in the modelling of plane wave scattering by a flat pre-fractal system of impedance strips. *IET Microw. Antennas Propag.* **2021**, *15*, 1310–1317. [CrossRef]
20. Lucido, M. Electromagnetic scattering from a graphene disk: Helmholtz-Galerkin technique and surface plasmon Resonances. *Mathematics* **2021**, *9*, 1429. [CrossRef]
21. Lucido, M. Helmholtz–Galerkin regularizing technique for the analysis of the THz-range surface-plasmon-mode resonances of a graphene microdisk stack. *Micro* **2022**, *2*, 295–312. [CrossRef]
22. Dukhopelnykov, S.V.; Lucido, M.; Sauleau, R.; Nosich, A.I. Circular dielectric rod with conformal strip of graphene as tunable terahertz antenna: Interplay of inverse electromagnetic jet, whispering gallery and plasmon effects. *IEEE J. Sel. Top. Quantum Electron.* **2021**, *27*, 4600908. [CrossRef]

23. Kaliberda, M.E.; Lytvynenko, L.M.; Pogarsky, S.A. Scattering of eigenmodes of planar dielectric waveguide with PEC wall by graphene strip grating at THz. *Waves Random Complex Media* **2021**. [CrossRef]
24. Kaliberda, M.E.; Lytvynenko, L.M.; Pogarsky, S.A. THz waves scattering by finite graphene strip grating embedded into dielectric slab. *IEEE J. Quantum Electron.* **2020**, *56*, 8500107. [CrossRef]
25. Kaliberda, M.E.; Lytvynenko, L.M.; Pogarsky, S.A.; Sauleau, R. Excitation of guided waves of grounded dielectric slab by a THz plane wave scattered from finite number of embedded graphene strips: Singular integral equation analysis. *IET Microw. Antennas Propag.* **2021**, *15*, 1171–1180. [CrossRef]
26. Kaliberda, M.E.; Pogarsky, S.A.; Sierhieieva, A.A. Integral equations in the H-polarized wave scattering from metasurface formed by finite multilayer graphene strip grating inside grounded dielectric slab. *Opt. Quantum Electron.* **2023**. [CrossRef]
27. Gandel, Y.V.; Polyanskaya, T.S. Justification of a numerical method for solving systems of singular integral equations in diffraction grating problems. *Differ. Equ.* **2003**, *39*, 1295–1307. [CrossRef]
28. Hanson, G.W. Dyadic Green's functions and guided surface waves for a surface conductivity model of graphene. *J. Appl. Phys.* **2008**, *103*, 064302. [CrossRef]
29. Hanson, G.W. Dyadic Green's functions for an anisotropic, non-local model of biased graphene. *IEEE Trans. Antennas Propagat.* **2008**, *56*, 747–757. [CrossRef]
30. Gomez-Diaz, J.S.; Mosig, J.R.; Perruisseau-Carrier, J. Effect of spatial dispersion on surface waves propagating along graphene sheets. *IEEE Trans. Antennas Propag.* **2013**, *61*, 3589–3596. [CrossRef]
31. Guillemin, E.A. *Communication Network*; John Wiley and Sons Inc.: London, UK, 1935; Volume 1.
32. Lifanov, I.K. *Singular Integral Equations and Discrete Vortices*; VSP: Utrecht, The Netherlands, 1996.
33. Kaminow, I.P.; Mammel, W.L.; Weber, H.P. Metal-clad optical waveguides: Analytical and experimental study. *Appl. Opt.* **1974**, *13*, 396–405. [CrossRef] [PubMed]
34. Svezhentsev, A.Y.; Nosich, A.I.; Volski, V.; Vandenbosch, G.A.E. THz range natural modes and scattering resonances of circular dielectric micro-cylinder covered with graphene: The H-polarization case. *Opt. Quantum Electron.* **2023**, *55*, 253. [CrossRef]